Analyst

ROYAL SOCIETY OF CHEMISTRY

PAPER

View Article Online
View Journal

Cite this: DOI: 10.1039/d0an00315h

A highly efficient preconcentration route for rapid and sensitive detection of endotoxin based on an electrochemical biosensor

Wenrui Ma,[a,b] Lulu Liu,[b,c] Yi Xu,[a,c,b] Li Wang,[a,b] Li Chen,[a,b] Sheng Yan,[d] Lingling Shui,[e] Zhijun Wang[f] and Shunbo Li *[a,b]

An impedimetric aptasensor for the detection of endotoxin in a microfluidic chip was proposed, in which the Apt/AuNPs/SPCE sensing surface was fabricated in a screen-printed electrode with good biological activity and stability. The quantitative detection of endotoxin was accomplished by electrochemical impedance spectroscopy (EIS) measurement before and after exposing to samples. The impedance biosensor offers an ultrasensitive and selective detection of endotoxin down to 500 pg mL^{-1} with a wide linear range from 500 pg mL^{-1} to 200 ng mL^{-1}. According to the Langmuir isotherm model, the interactions between the target molecules and the sensing surface had been analyzed and strong binding was concluded. Compared to the traditional static incubation methods, the microfluidic biosensor realizes the enrichment of endotoxin owing to the confined space and continuous flow nature, so that the lowest detection concentration is reduced from 5 ng mL^{-1} to 500 pg mL^{-1}, which is much lower than the existing technology, and the total assay time is shortened from 1.0 h to 0.5 h. The proposed microfluidic impedance biosensor provides a new strategy for the design of an aptasensor to realize the rapid detection of target biomolecules with high sensitivity and it can be integrated into wearable medical devices due to its flexible properties.

Received 12th February 2020,
Accepted 3rd May 2020

DOI: 10.1039/d0an00315h

rsc.li/analyst

Introduction

Endotoxin, often known as lipopolysaccharide (LPS), is a highly toxic component that is embedded in the outer cell wall membrane of most Gram-negative bacteria (GNB).[1] It is released into the environment during every phase of the bacterial growth cycle. A larger amount of endotoxin is released from dead bacteria cells and a small amount of endotoxin is released during their normal metabolism.[2,3] Endotoxin is ubiquitous in water, soil and air, and has an adverse health impact on humans and even small quantities of endotoxin injected into the human body can cause fever, septic shock and death.[4–6] For this reason, endotoxin is of paramount significance in the pathophysiology of many disease processes, such as microcirculation disturbance, septic shock, fever reaction, disseminated intravascular coagulation, *etc.*[7] Human beings are extremely sensitive to endotoxin. Elin *et al.* reported that the minimum intravenous pyrogenic dose of the reference *E. coli* endotoxin was only 0.1–0.5 ng kg^{-1}.[8] Recently, Bidne *et al.* reported that endotoxin exposure could affect female reproductive function.[9] Endotoxin contamination in urban domestic water also attracted people's concern. According to a report by Pouria *et al.* in 1998, 126 patients developed signs and symptoms of neurotoxicity and subacute hepatotoxicity, of which 60 patients died because of the contaminated municipal water after taking local lake water containing cyanobacteria as feed water in purified hemodialysis water.[10]

Thus, to avert a serious and wide range of health risks and even death triggered by endotoxin, the detection of endotoxin is urgently required by the Food and Drug Administration in many countries. Currently, the Limulus amebocyte lysate (LAL) assay is the most widely used method for quantitative detection of endotoxin in clinics.[11,12] However, the conventional LAL assay has been restricted in further applications due to the inevitable shortcomings such as low reproducibility, slow

[a]*Key Disciplines Lab of Novel Micro-Nano Devices and System Technology & Key Laboratory of Optoelectronic Technology and Systems (Ministry of Education), College of Optoelectronic Engineering, Chongqing University, Chongqing 400044, China. E-mail: shunbo.li@cqu.edu.cn*
[b]*International R & D center of Micro-nano Systems and New Materials Technology, Chongqing University, Shapingba, Chongqing 400044, China*
[c]*School of Chemistry and Chemical Engineering, Chongqing University, Chongqing 400044, China*
[d]*Institute for Advanced Study, Shenzhen University, Shenzhen 518060, P. R. China*
[e]*Guangdong Provincial Key Laboratory of Optical Information Materials and Technology, South China Normal University, Guangzhou 510631, China*
[f]*State Key Laboratory of Solidification Processing, Northwestern Polytechnical University, Xi'an 710072, People's Republic of China*

response, elaborated experimental setup and high cost.[13] Although other endotoxin biosensors based on the antibody–antigen specific recognition have been developed, they still have some unavoidable drawbacks such as high dependency on temperature, long incubation time and process time to obtain the results and being expensive, and the process of extracting antibodies from animal bodies is complicated and time-consuming.[14–16]

Fortunately, the highest affinity bio-receptor to endotoxin such as aptamers, peptides and enzymes has been gradually investigated and developed, which provided an alternative platform to construct biosensors for endotoxin detection.[17–21] Su *et al.* developed an impedance biosensor using DNA aptamers as the recognition elements.[22] Bai *et al.* developed a signal-on electrochemical aptasensor for endotoxin detection using DNA junction-aided enzymatic recycling and a graphene nanohybrid for amplification.[23] Liu *et al.* utilized a molecularly imprinted nano-membrane (MIM) and natural antibody as affinity molecules to fabricate a nanobiocomposite immunosensor for endotoxin determination.[24] These biosensors have high selectivity for endotoxin due to the high affinity to aptamers, peptides and enzymes, but they require a considerable incubation time of about 1 h, which will restrict the application of these biosensors to a certain extent. To shorten the incubation process of endotoxin, Brosel-Oliu *et al.* constructed a biosensor that could detect bacterial endotoxin within 20 minutes, and the limit of detection was 2 μg mL^{-1}.[25] The proposed biosensor was modified with PEI-(Con A-glycogen)$_2$-Con A multilayers that were able to prevent more efficient non-specific interactions of polyethyleneimine (PEI) and to ensure the selective biorecognition of LPS by Con A. But the detection limit of this method (2 μg mL^{-1}) is not comparable with that of the Limulus amebocyte lysate (LAL) assay, which will hardly meet the requirements. To lower the detection limit, researchers had made great efforts. Mayall *et al.* developed an electrochemical aptasensor for endotoxin detection by immobilizing Toll-Like receptor-4 (TLR-4) on a gold electrode and the limit of detection was 1 ng mL^{-1}.[26] Zandieh *et al.* constructed a silver-based localized surface plasmon resonance (LPSR) biosensor for endotoxin detection, and the limit of detection was lowered to be 340 pg mL^{-1} for endotoxin released from *E. coli*.[27] Shen *et al.* reported a ratiometric electrochemical aptasensor based on a target-induced cyclic amplification strategy for endotoxin detection, and the limit of detection was as low as the fg mL^{-1} level.[28] Although the detection limit of these methods had met most needs in clinics, the shortcomings were also obvious, such as long assay time, large instrumentation, large sample demand and so on, which limited their further applications.

Currently, due to their small sample consumption, rapid analysis speed, low cost, miniaturization, integration and portability, microfluidic biosensors have enormous potential for the detection of various biomarkers.[29–32] When they are used for the detection of biomolecules, such as glucose, uric acid and cancer biomarkers, electrochemical detection based on screen-printed or paper-based biosensors has attracted a lot of attention because of its unique advantages of portability, disposability and low cost.[33] Other than the mentioned unique properties of microfluidic biosensors, the confined space of the device itself would greatly enhance the electric related forces such as van der Waals forces[34,35] and electrokinetic forces,[36–39] which has been widely applied in self-assembly and manipulation of a small amount of fluid and microparticles in microfluidic devices. Thus, it may provide us the insight to take advantage of these effects.

In the present work, in order to meet the market's demand for portable, fast and highly sensitive detection devices, a simple and convenient microfluidic impedance biosensor for rapid and sensitive detection of endotoxin was designed and the effect of microchannels on preconcentration was comprehensively investigated. The microfluidic biosensor mainly consisted of two parts, the modified screen-printed carbon electrode (SPCE) for specific biorecognition of endotoxin, and the microfluidic channel for dynamic enrichment of endotoxin. The sensing surface was fabricated by the strong affinity of 5′ end amino groups of the aptamer (Apt) with Au nanoparticles (AuNPs). The covalent binding between 5′ end amino groups of Apt and AuNPs produced a highly steady Apt/AuNPs/SPCE sensing surface for endotoxin detection. To confirm the dynamic enrichment effect of the microfluidic biosensor on endotoxin, the detection of endotoxin under the traditional static incubation was also conducted and compared. Simultaneously, the maximum electron transfer impedance ($R_{et_{max}}$) was calculated by using the Langmuir isotherm model when the biosensor reached saturation.

Experimental

Materials and apparatus

Endotoxin and the DNA oligonucleotide (aptamer) 3′-CGATAGATTGTTGTAAGACAATCTTCC-5′-NH_2 were obtained from Sangon Biotech Co., Ltd (Shanghai, China). $K_3[Fe(CN)_6]$ and $K_4[Fe(CN)_6]$ were obtained from Chengdu Chemical Reagent Factory (Chengdu, China). KCl and D-glucose were purchased from Shanghai Macklin Biochemical Co., Ltd (Shanghai, China). Gold(III) chloride trihydrate ($AuCl_3 \cdot HCl \cdot 3H_2O$) was purchased from Aikon (Jiangsu, China). Ascorbic acid (AA) was obtained from Chengdu Kelong Chemical Reagent Factory (Chengdu, China). Bovine serum albumin (BSA) was purchased from Sigma (Chongqing, China). A poly(dimethylsiloxane) (PDMS) prepolymer and a curing agent (Sylgard 184 silicone elastomer) were purchased from Dow Corning (Wiesbaden, Germany). The water for the bacterial endotoxin test for the preparation of endotoxin standard solution was purchased from Zhanjiang Bokang Marine Biological Co., Ltd (Guangdong, China). All solutions were prepared using deionized distilled water with a resistivity of 18.2 MΩ cm through a Millipore MilliQ water purification system. All chemicals were of analytical grade and used as received.

The electrochemical impendence spectroscopy (EIS) test was performed on a VersaSTAT3 Potentiostat (Princeton

applied research, USA) and cyclic voltammetry (CV) was performed using a CHI 660E electrochemical workstation (CH Instruments Inc.). EIS and CV were carried out in a portable screen printed carbon electrode (SPCE) consisting of a polyethylene terephthalate (PET) substrate, a carbon working electrode (4 mm diameter), a carbon auxiliary electrode, and an Ag/AgCl reference electrode. The morphology of the sensor surface was characterized using an Ultra High Resolution Field Emission Scanning Electron Microscope (JSM-7800F, NEC Electronics Corporation, Japan).

Fabrication of the Apt/AuNPs/C modified electrode

Before modification, the SPCE surface was first electrochemically activated by performing the CV scan (20 cycles) in 0.5 M dilute sulfuric acid with a potential range from −0.6 V to +0.8 V and a scan rate of 50 mV s^{-1}. This was followed by cleaning of the electrode in DI water and drying in air. The Apt/AuNP modified carbon working electrode was prepared by means of electrochemical deposition of $HAuCl_4$ solution and molecular binding. First, AuNPs on the SPCE surface were obtained by electrochemical deposition of 10 mM $HAuCl_4$ and 75 mM KCl aqueous solution at a constant potential of −0.75 V for 300 s. Then 30 μL of 1 μM aptamer was immobilized on the AuNPs/SPCE by drop casting and kept overnight. The electrode was again washed with DI water to remove the unbound aptamer and the Apt/AuNPs/C electrode was dried in air. Furthermore, in order to avoid the nonspecific binding of the analyte, the Apt/AuNPs/SPCE was immersed in 1 mM BSA for 1 min following the reported method,[13] and again rinsed with DI water and dried in air. A schematic diagram depicting the fabrication is illustrated in Fig. 1(a).

Detection procedures

A series of various concentrations of endotoxin solutions in the range from 100 pg mL^{-1} to 1 μg mL^{-1} were prepared for testing. The detection procedures and the illustration of endotoxin capture by the sensing surface are shown in Fig. 1(b) and (c). Before quantitative electrochemical measurements, the enrichment of endotoxin was achieved using a simple microfluidic chip, which had two layers, the Apt/AuNPs/SPCE sensing surface modified on the screen printed carbon electrode as the bottom layer, and the PDMS cover with a microcavity (diameter of 4 mm) and a microchannel (length 7.5 mm, width 0.8 mm and height 0.2 mm) as the top layer. Different concentrations of endotoxin with volumes of 30 μL were pumped at a constant flow rate of 1 μL min^{-1} through the microfluidic chip, so as to achieve rapid enrichment of endotoxin. As a comparison, the traditional static incubation of endotoxin referred to dispensing a certain amount of endotoxin sample to the sensing surface. According to previously reported literature,[25,40] the time for static incubation to capture target molecules by the aptamer is longer than 1.0 h at room temperature. Therefore, the traditional static incubation of endotoxin with an incubation time of 1.0 h was employed as a control experiment. Electrochemical impedance spectroscopy (EIS) was used for the quantitative detection of endotoxin. In the EIS measurement, a sine wave with an amplitude of 10 mV was applied to a carbon working electrode in the frequency range from 0.1 Hz to 100 kHz and 2 mM $[Fe(CN)_6]^{3-/4-}$ in 10 mM pH 7.4 phosphate buffer saline (PBS) containing 137 mM NaCl and 2.7 mM KCl was used as the electrolyte.

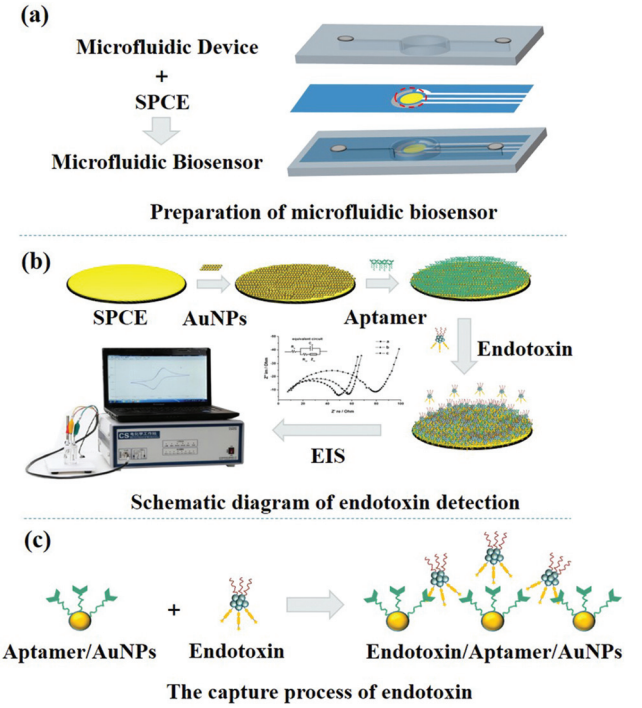

Fig. 1 (a) Schematic illustration of the structure and preparation process of the microfluidic biosensor; (b) schematic diagram of endotoxin detection; (c) the capture process of endotoxin by the sensing surface.

Results and discussion

Characterization of Apt/AuNPs/C

The properties of sensing surface Apt/AuNPs/SPCE were characterized by SEM and EIS and are shown in Fig. 2. The electrochemical deposition of AuNPs is of great significance for this sensor preparation. The SEM image of AuNPs on the SPCE in Fig. 2(a) shows that the AuNPs are uniformly distributed on the SPCE surface. The Nyquist plots of the biosensor including a semicircle portion at high frequencies corresponding to the electron-transfer-limited process and a linear part at low frequencies representing the diffusion-limited process are indicated in Fig. 2(b). Electron transfer impedance (R_{et}) is the most sensitive constituent part to indicate the physical, chemical and biomass changes on the sensing surface. In our study, the equivalent circuit is fitted with ZsimWin software. After modification of AuNPs, a larger semicircle on a bare carbon electrode disappears in the Nyquist plots which means that AuNPs are formed on the surface of the electrode. Followed by the incubation of the aptamer with 5′ end amino groups and the AuNPs/SPCE surface for

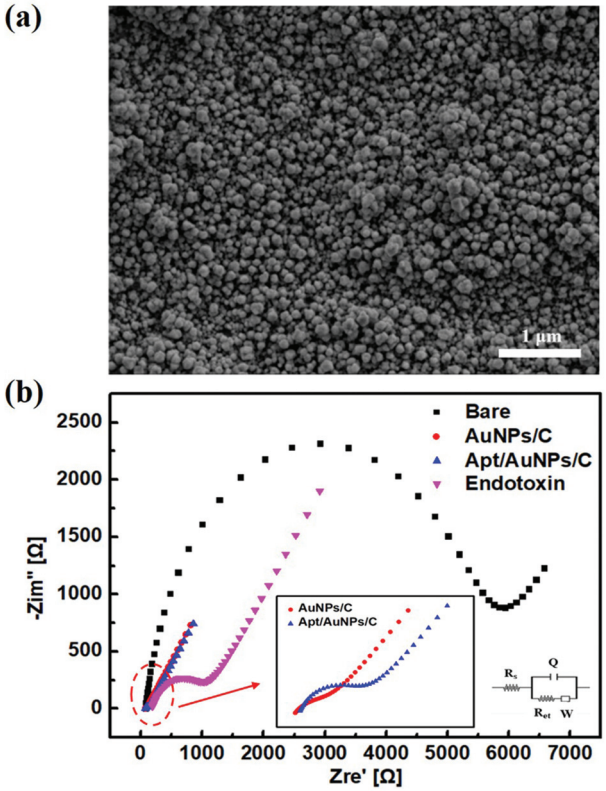

Fig. 2 (a) SEM image of AuNPs on the SPCE deposited by the electrochemical method; (b) EIS measurement (Nyquist plots) of the biosensor during the preparation process and the inset representing the magnified views before and after aptamer immobilization.

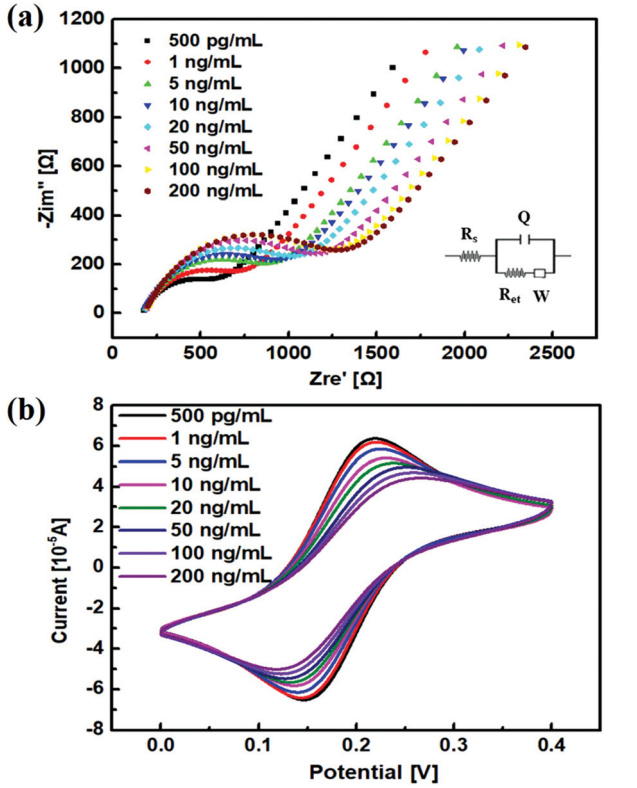

Fig. 3 The EIS measurements (a) and cyclic voltammetry measurements (b) of the designed biosensor after exposing to endotoxin with various concentrations.

12 hours, it is found that the R_{et} value shows a slightly rising trend (the inset of Fig. 2(b)). However, an obvious semicircle at high frequencies emerges and the R_{et} value is increased significantly after endotoxin capture, implying its capability to employ electrochemical impedance spectroscopy to detect endotoxin.

Performance of the designed biosensor

The EIS measurements of endotoxin at various concentrations using the designed microfluidic biosensor were conducted and the results are depicted in Fig. 3(a). With the successive increase of endotoxin concentration, the semicircle portion at high frequencies representing the electron-transfer-limited process is gradually larger, indicating that the value of R_{et} controlled by the electron-transfer-limited process is dramatically influenced by the selective recognition of endotoxin molecules on the sensing surface by the aptamer. This remarkable enhancement of the R_{et} value can be attributed to the insulating property of the interface caused by the specific binding of the target endotoxin molecule, which would slowdown the oxidation/reduction of the $[Fe(CN)_6]^{3-/4-}$ in the sample. The recognition of endotoxin with the aptamer immobilized on the AuNPs/SPCE was further demonstrated by cyclic voltammetry (CV) in the range of 0–0.4 V, as shown in Fig. 3(b). As reported, many CV measurements were conducted in the range of −0.2 V–0.6 V. A shorter range was chosen in this study to decrease the analysis time and this range was enough to show the change of peaks at different endotoxin concentrations. It could be observed that the peak current decreased upon increasing the endotoxin concentration, making it clear that the steric hindrance effect at the interface produced by endotoxin indeed exists. On the basis of the above results, it is confirmed that the electrochemical impedance method using the designed microfluidic biosensor has the capability to detect endotoxin.

The quantitative detection of target endotoxin is significant in evaluating the degree of pathogen infection in clinical tests. Therefore, the electron transfer impedance (R_{et}) is calculated according to the EIS measurement in Fig. 3(a) and the relationship between R_{et} and logarithm of concentration is plotted and shown in Fig. 4. A linear curve was obtained under endotoxin concentration from 500 pg mL^{-1} to 200 ng mL^{-1} with a correlation coefficient of 0.9978. The results indicate that the limit of detection of endotoxin concentration could be achieved as low as 500 pg mL^{-1} and the good linearity ensures the precise determination of endotoxin concentration in the test sample.

The performance of various biosensors used for endotoxin detection is summarized in Table 1. In comparison with the reported methods, the detection limit offered by the present method is much lower than that of most technologies.

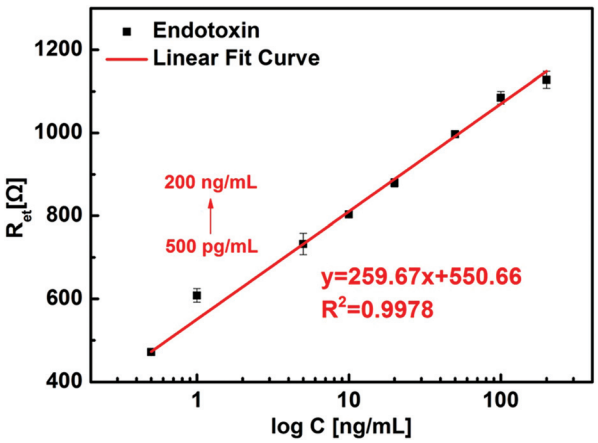

Fig. 4 Linear relationship between the electron transfer impedance and logarithmic value of endotoxin concentration.

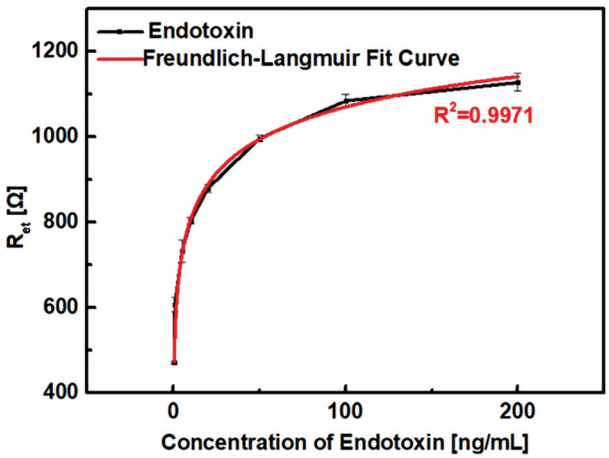

Fig. 5 Plots of the electron transfer impedance *versus* endotoxin concentration.

Table 1 Detection limit and assay time for endotoxin

Technique	Sensing surface	LOD (ng mL^{-1})	Assay time (min)	Ref.
Luminescence	MIM	4.0	60	24
EIS	Con A	2000	20	25
EIS	TLR-4/Au	1.0	—	26
LSPR	PmB	0.34	60	27
CV	FcPmB	2.0	—	41
EIS	Apt/AuNPs	0.5	30	This work

MIM: imprinted nano-membrane; Con A: concanavalin A; TLR-4: human toll-like receptor-4; LSPR: localized surface plasmon resonance; PmB: polymyxin B; FcPmB: ferrocene labeled polymyxin B.

Moreover, the microfluidic impedance biosensor can perform with rapid analysis speed along with high precision when compared with other reported biosensors for endotoxin detection.

Interactions between the aptamer and endotoxin

In previously reported works, little attention has been paid to the capture process of endotoxin by an aptamer. To further understand the interactions between the biosensor surface and endotoxin molecule, the isotherm adsorption model is adopted to establish the relationship between the adsorption quantity of endotoxin and the concentration of endotoxin in the sample solution. The Langmuir isothermal adsorption model was widely applied in various binding processes such as the cancer cells to aptamers,[42] pathogenic bacteria and mannose to aptamers.[43] Thus, the Langmuir isothermal adsorption model was also applied for analyzing the binding of endotoxin to aptamers. The frequently used Freundlich–Langmuir isotherm adsorption model can be expressed as follows:[44,45]

$$q_e = q_{max} \cdot \frac{K_D \cdot [C_e]^{1/n}}{1 + K_D[C_e]^{1/n}} \quad (1)$$

where q_e is the adsorption quantity of molecules under the equilibrium state, and q_{max} stands for the maximum adsorption capacity of molecules by the constructed sensor. K_D represents the adsorption coefficient, which is related to temperature and absorbent types. $[C_e]$ is the concentration of target molecules in the solution under the equilibrium state. $1/n$ refers to the strength of binding affinity, where the value smaller than one implies a strong binding affinity belonging to the chemisorption process and the value larger than one is an indication of cooperative adsorption.

Fig. 5 depicts the relationship between R_{et} and the concentration of endotoxin. As can be seen from the plot, R_{et} has a rapid growth relationship at lower endotoxin concentration, while it gradually reaches the saturation state at higher endotoxin concentration. This relationship between R_{et} and the concentration of endotoxin has a typical trend associated with the Langmuir isotherm model. The adsorption quantity of endotoxin q_e is closely related to the electron transfer impedance on the electrode surface; therefore the q_e can be replaced by R_{et} and q_{max} is substituted with $R_{et_{max}}$. The saturation of the electron transfer impedance as the concentration of endotoxin increases is caused by the full coverage of active sites (aptamer) on the sensing surface by endotoxin during incubation. The red line in Fig. 5 has been fitted by eqn (1) with a correlation coefficient of 0.9971, indicating that the process of special recognition and capture of endotoxin is in agreement with the Freundlich–Langmuir isotherm model. The fitting results show that the values of $R_{et_{max}}$, K_D and $1/n$ are (1619 ± 223), (0.51 ± 0.11) and (0.71 ± 0.03), respectively. The value of $1/n$ is smaller than one, which indicates that it is a chemisorption process rather than a physisorption process, and further indicates that the aptamer had a strong binding affinity to endotoxin molecules.

Comparison between traditional static incubation and microfluidic enrichment

The electrostatic force and van der Waals force are associated with the adsorption process. The freely moving endotoxin molecules due to Brownian motion can be attracted by the

sensing surface by electrostatic force in the vicinity within the range on the order of micrometer which is the effective working distance of electrostatic force. With the increase of distance, the electrostatic force decreases rapidly. Therefore, for the traditional static incubation method, the sensing surface can only adsorb endotoxin near it, the molecules a bit far away from the surface have to diffuse into the working region before binding and this process took time to finish. In contrast, with the help of the small size of microfluidic channel (200 μm) in the present design, almost all endotoxin molecules are confined in the working region of electrostatic force and the adsorption is more effective than the traditional incubation. Moreover, the fluid flow in the microfluidic device can enhance the collision between endotoxin and aptamer, promoting the adsorption again. As comparison, the incubation process using a microfluidic chip is called dynamic incubation. Thus, the time for dynamic incubation is shortened compared to static incubation by eliminating the requirement of a long diffusion distance in the working region of electrostatic force and the continuous flow in the microfluidic device is actually the enrichment of endotoxin from low concentration in the sample to the sensing surface. It is noted that the total sample volume used in dynamic incubation by the microfluidic device is the same as that used in the traditional static incubation. Consequently, the shorter incubation time and the lower detection limit are achieved by the microfluidic biosensor. The schematic diagram depicting the binding between endotoxin and the sensing surface by static incubation and dynamic enrichment using the microfluidic device is shown in Fig. 6.

In order to demonstrate the differences of actual performance between dynamic incubation and the traditional static incubation for endotoxin detection, sample solutions with a range of endotoxin concentrations (0.5 ng mL^{-1}, 1 ng mL^{-1}, 5 ng mL^{-1}, and 10 ng mL^{-1}) were prepared, incubated and measured repeatedly 3 times. The changes of electron transfer impedance before and after exposing to endotoxin are shown in Fig. 7. It is clearly seen that the dynamic incubation method using the designed microfluidic biosensor has larger change of electron transfer impedance, which confirms our prediction that the microfluidic method can effectively enrich the endotoxin molecules. The detection limit is lower and the incubation time is shorter than that of the traditional static incubation method.

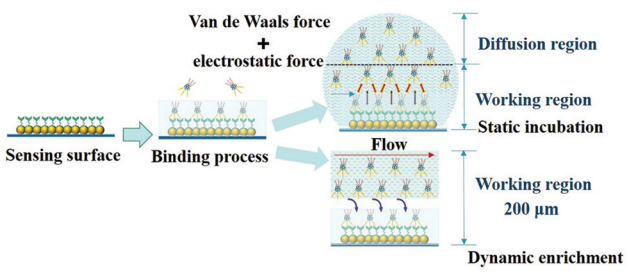

Fig. 6 Schematic diagram depicting the binding between endotoxin and the sensing surface by static incubation and dynamic enrichment using the microfluidic device.

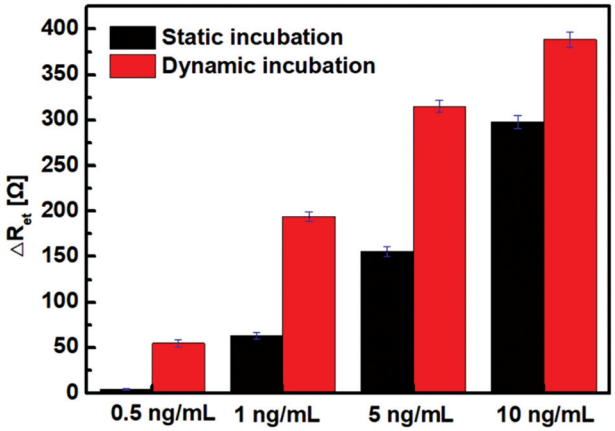

Fig. 7 The histogram showing the change of electron transfer impedance before and after exposing to endotoxin with concentrations of 0.5 ng mL^{-1}, 1 ng mL^{-1}, 5 ng mL^{-1} and 10 ng mL^{-1}. The black posts represent the static incubation and the red posts represent the dynamic incubation using the designed microfluidic chip.

The enrichment strategy for a biosensor is very effective in detecting biomolecules in ultra-low concentrations. Recently, Sanjay *et al.* reported the novel design of the detection protocol using flowing back-and-forth of sample through a portable and plug-and-play paper substrate within the microfluidic channels. It enabled the enhancement of biomarker adsorption and further the sensitivity was improved and the assay time was decreased.[46] This standpoint is in agreement with the enrichment technique proposed in our study. The reported work is suitable in ELISA assay which is based on the paper microfluidics and colorimetric measurement, while our method is helpful to enrich biomolecules for the biosensor using an electrochemical method for detection. Thus, the presented method provides a new strategy for the preconcentration of target biomolecules to realize rapid and highly sensitive detection in microfluidic devices using an electrochemical method.

Selectivity of the biosensor

To verify the specificity of the prepared biosensor, D-glucose, ascorbic acid (AA) and bovine serum albumin (BSA) were chosen as interfering substances, which represented the common glucose, proteins and other small molecules present in the detection samples such as blood, to evaluate the selectivity. To demonstrate the robustness of the biosensor, the concentration of interfering substances was chosen to be 100 ng mL^{-1}, which was 100 times larger than that of endotoxin. After exposing the biosensor to the prepared samples using the developed microfluidic enrichment method, the R_{et} variations from EIS responses of the microfluidic biosensor were recorded and the results of 3 measurements are shown in Fig. 8. It is clearly seen that there are almost no differences in R_{et} change after exposing to high concentrations of D-glucose,

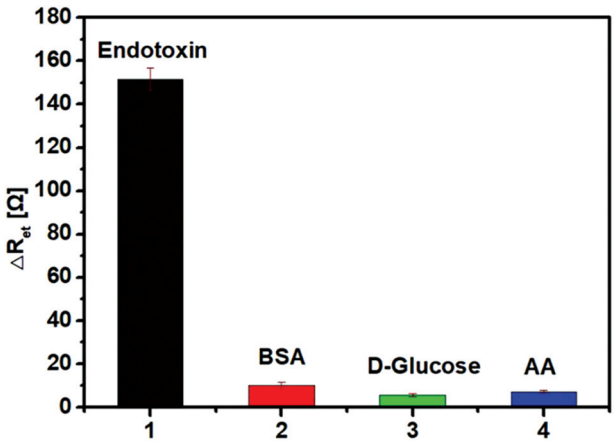

Fig. 8 The electron transfer impedance changes after exposing to 1 ng mL^{-1} endotoxin, 100 ng mL^{-1} BSA, 100 ng mL^{-1} D-glucose and 100 ng mL^{-1} AA.

ascorbic acid (AA) and bovine serum albumin (BSA). In contrast, the presence of endotoxin in the sample solution has an obvious R_{et} change. It is concluded that the immersion in BSA for 1 min is enough to block nonspecific binding and the designed Apt/AuNPs/C biosensor has a good selectivity for endotoxin over other biomolecules.

Conclusions

In this study, a novel and simple microfluidic impedance biosensor for the selective and sensitive detection of endotoxin had been developed. The prepared biosensor could successfully detect target endotoxin down to 500 pg mL^{-1} with a wide linear range from 500 pg mL^{-1} to 200 ng mL^{-1}. Compared with traditional static incubation, the dynamic incubation of target endotoxin by a simple microfluidic device lowered the detection limit from 5 ng mL^{-1} to 500 pg mL^{-1} and shortened the whole assay time from 1 h to 0.5 h since the confined microchannel led the molecules to bind to the sensing surface by electrostatic force and van der Waals force. Compared to the traditional bulk detection system, in which the sensing surface has a limited area and working distance for target molecule binding, resulting in diffusion and adsorption in the bulk solutions taking a long time, the use of a confined microchannel and continuous flow forced the target molecules to bind to the sensing surface for fast preconcentration to enhance the sensitivity and shorten the detection time. The detection limit was much lower than that of the existing technology. According to the fitting analysis of Langmuir isotherm adsorption, the interaction between endotoxin molecules and aptamers has a strong binding force, which is beneficial for the designed biosensor. The selectivity test confirmed the noninterference by proteins, glucose and other biomolecules. The proposed microfluidic impedance biosensor provided a new strategy for the design of aptasensors to realize the rapid and sensitive detection of target biomolecules with simple operation and instrumentation.

Conflicts of interest

There are no conflicts to declare.

Acknowledgements

This work was supported by the Fundamental Research Funds for the Central Universities (2018CDGFGD0010, 2019CDYGYB003, and 2019CDXYGD0028), the National Natural Science Foundation of China (61904021 and 61971074), Guangdong Provincial Key Laboratory of Optical Information Materials and Technology (2017B030301007), the Fund of the State Key Laboratory of Solidification Processing in NWPU, (Grant No. SKLSP201907), the pre-research foundation (31513070102-1), and the Key project of science and technology research program of Chongqing Education Commission of China (KJ201900138894836).

Notes and references

1 J. Jackie, W. K. Lau, H. T. Feng and S. F. Y. Li, *Crit. Rev. Anal. Chem.*, 2019, **49**, 126–137.
2 C. Zhang, F. Tian, M. Zhang, Z. Zhang, M. Bai, G. Guo, W. Zheng, Q. Wang, Y. Shi and L. Wang, *Sci. Total Environ.*, 2019, **681**, 365–378.
3 O. Schlosser, A. Huyard and V. Catalan, *Water Sci. Technol.*, 2011, **64**, 1073–1080.
4 M. S. Trent, C. M. Stead, A. X. Tran and J. V. Hankins, *J. Endotoxin Res.*, 2006, **12**, 205–223.
5 R. L. Danner, R. J. Elin, J. M. Hosseini, R. A. Wesley, J. M. Reilly and J. E. Parillo, *Chest*, 1991, **99**, 169–175.
6 S. E. Kim, W. Su, M. Cho, Y. Lee and W. S. Choe, *Anal. Biochem.*, 2012, **424**, 12–20.
7 R. B. Yang, M. R. Mark, A. Gray, A. Huang, M. H. Xie, M. Zhang, A. Goddard, W. I. Wood, A. L. Gurney and P. J. Godowski, *Nature*, 1998, **395**, 284–288.
8 R. J. Elin, S. M. Wolff, K. McAdam, L. Chedid, F. Audibert, C. Bernard and F. Oberling, *J. Infect. Dis.*, 1981, **144**, 329–336.
9 K. L. Bidne, M. J. Dickson, J. W. Ross, L. H. Baumgard and A. F. Keating, *Reproduction*, 2018, **155**, R169–R181.
10 S. Pouria, A. de Andrade, J. Barbosa, R. L. Cavalcanti, V. T. S. Barreto, C. J. Ward, W. Preiser, G. K. Poon, G. H. Neild and G. A. Codd, *Lancet*, 1998, **352**, 21–26.
11 K. G. Ong, J. M. Leland, K. Zeng, G. Barrett, M. Zourob and C. A. Grimes, *Biosens. Bioelectron.*, 2006, **21**, 2270–2274.
12 K. Ito, K. Y. Inoue, K. Ino, T. Matsue and H. Shiku, *Analyst*, 2019, **144**, 3659–3667.
13 B. Posha, S. R. Nambiar and N. Sandhyarani, *Biosens. Bioelectron.*, 2018, **101**, 199–205.

14 W. Su, M. Lin, H. Lee, M. Cho, W. S. Choe and Y. Lee, *Biosens. Bioelectron.*, 2012, **32**, 32–36.
15 S. Voss, R. Fischer, G. Jung, K. H. Wiesmueller and R. Brock, *J. Am. Chem. Soc.*, 2007, **129**, 554–561.
16 L. Rivas, C. C. Mayorga-Martinez, D. Quesada-Gonzalez, A. Zamora-Galvez, A. de la Escosura-Muniz and A. Merkoci, *Anal. Chem.*, 2015, **87**, 5167–5172.
17 Y. Chen and R. M. Corn, *J. Am. Chem. Soc.*, 2013, **135**, 2072–2075.
18 J. Niu, X. Hu, W. Ouyang, Y. Chen, S. Liu, J. Han and L. Liu, *Anal. Chem.*, 2019, **91**, 2360–2367.
19 R. Saravanan, D. A. Holdbrook, J. Petrlova, S. Singh, N. A. Berglund, Y. K. Choong, S. Kjellstrom, P. J. Bond, M. Malmsten and A. Schmidtchen, *Nat. Commun.*, 2018, **9**, 2762.
20 U. Ohto, K. Fukase, K. Miyake and T. Shimizu, *Proc. Natl. Acad. Sci. U. S. A.*, 2012, **109**, 7421–7426.
21 S. J. Ding, B. W. Chang, C. C. Wu, C. J. Chen and H. C. Chang, *Electrochem. Commun.*, 2007, **9**, 1206–1211.
22 W. Su, M. Cho, J. D. Nam, W. S. Choe and Y. Lee, *Electroanalysis*, 2013, **25**, 380–386.
23 L. Bai, Y. Chai, X. Pu and R. Yuan, *Nanoscale*, 2014, **6**, 2902–2908.
24 C. Liu, J. Y. Xu, J. F. Qi, Y. J. Liu, J. W. Kang, H. Y. Wang, S. Y. Chen, Z. Huang and B. Lu, *Sens. Actuators, B*, 2019, **290**, 1–8.
25 S. Brosel-Oliu, D. Galyamin, N. Abramova, F.-X. Munoz-Pascual and A. Bratov, *Electrochim. Acta*, 2017, **243**, 142–151.
26 R. M. Mayall, M. Renaud-Young, N. W. C. Chan and V. I. Birss, *Biosens. Bioelectron.*, 2017, **87**, 794–801.
27 M. Zandieh, S. N. Hosseini, M. Vossoughi, M. Khatami, S. Abbasian and A. Moshaii, *Anal. Biochem.*, 2018, **548**, 96–101.
28 W. Shen, Y. Zhuo, Y. Chai and R. Yuan, *Anal. Chem.*, 2015, **87**, 11345–11352.
29 X. Wei, W. Zhou, S. T. Sanjay, J. Zhang, Q. Jin, F. Xu, D. C. Dominguez and X. Li, *Anal. Chem.*, 2018, **90**, 9888–9896.
30 M. Dou, S. T. Sanjay, D. C. Dominguez, S. Zhan and X. Li, *Chem. Commun.*, 2017, **53**, 10886–10889.
31 M. Dou, J. M. Garci Jr., S. Zhan and X. Li, *Chem. Commun.*, 2016, **52**, 3470–3473.
32 M. Dou, N. Macias, F. Shen, J. D. Bard, D. C. Dominguez and X. Li, *EClinicalMedicine*, 2019, **8**, 72–77.
33 K. S. Prasad, X. Cao, N. Gao, Q. Jin, S. T. Sanjay, G. Henao-Pabon and X. Li, *Sens. Actuators, B*, 2020, **305**, 127516.
34 F. W. Delrio, M. P. De Boer, J. A. Knapp, E. D. Reedy, P. J. Clews and M. L. Dunn, *Nat. Mater.*, 2005, **4**, 629–634.
35 Y. Dou, B. Wang, M. Jin, Y. Yu, G. Zhou and L. Shui, *J. Micromech. Microeng.*, 2017, **27**, 113002.
36 T. M. Squires, *Lab Chip*, 2009, **9**, 2477–2483.
37 S. Li, M. Li, Y. S. Hui, W. Cao, W. Li and W. Wen, *Microfluid. Nanofluid.*, 2013, **14**, 499–508.
38 S. Li, M. Li, K. Bougot-Robin, W. Cao, I. Y. Y. Chau, W. Li and W. Wen, *Biomicrofluidics*, 2013, **7**, 024106.
39 S. Li, W. Cao, Y. S. Hui and W. Wen, *Nanoscale Res. Lett.*, 2014, **9**, 147.
40 Z. Li, F. Luo, G. Dai, Y. Lu, S. Ai, P. He and Q. Wang, *Microchem. J.*, 2019, **150**, 104178.
41 D. Kato, A. Oda, M. Tanaka, S. Iijima, T. Kamata, M. Todokoro, Y. Yoshimi and O. Niwa, *Electroanalysis*, 2014, **26**, 618–624.
42 M. Bakhshpour, A. K. Piskin, H. Yavuz and A. Denizli, *Talanta*, 2019, **204**, 840–845.
43 F. Cui, Y. Xu, R. Wang, H. Liu, L. Chen, Q. Zhang and X. Mu, *Biosens. Bioelectron.*, 2018, **103**, 94–98.
44 A. Gunay, E. Arslankaya and I. Tosun, *J. Hazard. Mater.*, 2007, **146**, 362–371.
45 K. Y. Foo and B. H. Hameed, *Chem. Eng. J.*, 2010, **156**, 2–10.
46 S. T. Sanjay, M. Li, W. Zhou, X. Li and X. Li, *Microsyst. Nanoeng.*, 2020, **6**, DOI: 10.1038/s41378-020-0143-5.

